Three-Dimensional Structure of Soybean Trypsin/Chymotrypsin Bowman–Birk Inhibitor in Solution†

Milton H. Werner and David E. Wemmer*

Chemical Biodynamics Division, Lawrence Berkeley Laboratory, and Department of Chemistry, University of California, Berkeley, Berkeley, California 94720

Received September 4, 1991; Revised Manuscript Received October 24, 1991

ABSTRACT: The three-dimensional structure of soybean trypsin/chymotrypsin Bowman–Birk inhibitor in solution has been determined by two-dimensional ^{1}H nuclear magnetic resonance spectroscopy and dynamical simulated annealing using the program XPLOR. The structure was defined by 907 NOEs involving intra- and interresidue contacts which served as distance constraints for a protocol of dynamical simulated annealing. In addition, 48 ϕ angle constraints involving non-proline amino acids, 29 χ angle constraints, six ω angle constraints for the X–Pro peptide bond, and 35 stereoassignments for prochiral centers were incorporated during the course of the calculation. The protein is characterized by two distinct binding domains for serine protease. Each domain is comprised of a β-hairpin (antiparallel β-sheet and a *cis*-proline-containing type VIb reverse turn) with a short segment making a third strand of antiparallel β-sheet. The structure determination and refinement are described, and the structure is compared to other structures of Bowman–Birk inhibitors as well as other families of serine protease inhibitors.

Bowman–Birk inhibitors (BBI) are small serine protease inhibitors (6–9 kDa) containing seven disulfide bonds. Among the families of serine protease inhibitors (Laskowski & Kato, 1980), BBI is unique in that it is capable of inhibiting 2 equiv of protease per equivalent of inhibitor at kinetically independent binding sites.

A number of isoforms of the Bowman–Birk type have been isolated, each being distinguished by its serine protease specificity. Classical BBI from soybeans (hereafter referred to as BBI-I) binds trypsin and chymotrypsin at distinct sites. It is comprised of 71 amino acids, and its secondary structure has recently been described (Werner & Wemmer, 1991).

Intrigued by the unique properties of BBI-I as a serine protease inhibitor, we embarked on an extended study of the structure of BBI-I and its interaction with serine protease. We report here the structure of BBI-I determined in an 18% acetonitrile/aqueous cosolvent. Analysis of the pattern and intensity of important secondary and tertiary NOE contacts in the presence and absence of acetonitrile indicated that the native protein structure was preserved in the cosolvent. The structure is compared to other structures of Bowman–Birk inhibitors determined by X-ray crystallography, and the general features of BBI-I are compared to other serine protease inhibitor families.

Materials and Methods

NMR Spectroscopy. The ^{1}H NMR assignments have previously been described in a recent report (Werner & Wemmer, 1991). All spectra were recorded with a Bruker AMX-600 equipped with digital phase shifters, a ^{1}H probe, and an X32 computer. All two-dimensional spectra were collected in the pure phase absorption mode utilizing the time-proportional phase incrementation (TPPI) technique (Redfield & Kunz, 1975; Drobny et al., 1978; Bodenhausen et al., 1980) as described by Marion and Wüthrich (1983). All spectra were processed using the program FELIX (version 1.1, Hare Research, Inc.).

For the analysis of interproton distance constraints involving the amide protons, NOESY spectra (Jeener et al., 1979; Macura et al., 1980) were recorded in 18% acetonitrile-d_3/H_2O (v/v) cosolvent (hereafter termed H_2O) at pH 5.0, 25 °C, and pH 5.7, 35 °C, 2 mM protein, using mixing times of 35, 40, 60, 125, and 200 ms. For the analysis of interproton distance constraints involving the nonexchangeable protons of the side chains, NOESY spectra were recorded in 18% acetonitrile-d_3/D_2O (99.9%) (hereafter termed D_2O), pH 5.7, at 25 and 35 °C using mixing times of 30, 40, and 100 ms. For NOESY spectra recorded in H_2O, the water resonance was suppressed by employing a "jump and return" sequence (90°–τ–90°, τ = 90 μs) (Plateau & Guéron, 1982) with phase cycling and processing according to Driscoll et al. (1989). For NOESY spectra recorded in D_2O, the residual water resonance was suppressed by selective irradiation during the relaxation delay and mixing time. In all NOESY spectra, the mixing time was randomly varied by 20% for spectra recorded with a mixing time less than 60 ms and by 10% otherwise to suppress peaks arising from zero-quantum coherence. Typically, NOESY spectra were recorded with 512 increments of 2K complex data except for one NOESY spectrum in H_2O and 60 ms for which 1024 increments of complex data were recorded.

$^3J_{N\alpha}$ coupling constants were analyzed in DQF-COSY spectra (pH 5.7, 35 °C) according to the technique of Kim and Prestegard (1989). $^3J_{\alpha\beta}$ coupling constants were analyzed qualitatively in DQF-COSY (Marion & Wüthrich, 1983) and measured from a P.E.COSY spectrum (Mueller, 1987) in D_2O. For P.E.COSY, 1024 increments of 2K complex data were collected at pH 5.7, 35 °C. The spectrum was zero-filled to yield a digital resolution of 1.36 Hz/point in ω_1 and ω_2.

Distance and Angle Constraints. The majority of distance constraints for NOEs involving the amide protons (650 in-

† This work was supported by the Office of Energy Research, Office of Health and Environmental Research, Health Effects Research Division of the U.S. Department of Energy under Contract No. DE-AC03-76 SF 00098, through the Instrumentation Grants DE FG05-86 ER 75281 from the U.S. Department of Energy and DMB 86-09035 and BBS 87-20134 from the National Science Foundation. Computational time was supported by the National Institutes of Health Grant 8SORROS61A to the Department of Chemistry Graphics Facility, University of California, Berkeley.

* To whom correspondence should be addressed.

0006-2960/92/0431-999$03.00/0

traresidue, sequential, and nonsequential NOEs) were derived from a single 60-ms NOESY spectrum in H_2O (35 °C, pH 5.7) and a single 40-ms NOESY spectrum in D_2O (35 °C, pH 5.7) for the analysis of the intraresidue NOEs involving side-chain protons. The experimental NOEs were classified according to strong (1.8–2.3 Å) (1.8–2.7 Å for NOEs involving backbone atoms and the amide proton), medium (1.8–3.3 Å, in a few cases extended to 3.5 Å), and weak (1.8–5.0 Å) intensities and corrected for center-averaging (equivalent to the use of pseudoatoms) as described by Wüthrich et al. (1983). In addition, 0.5 Å was added to the upper limit of distance constraints involving methyl groups to account for their higher intensity in NOESY spectra (Wagner et al., 1987; Clore et al., 1987). During the course of the calculation and analysis, additional constraints derived from 125- and 200-ms NOESY spectra (35 °C, pH 5.7) were included by comparison of distances derived from an initial family of 53 structures to NOESY spectra in order to resolve amibiguities in the NOE assignments.

In addition to these experimental distance constraints, the seven disulfide cross-links were defined by two additional distance constraints defining bond lengths and angles. These were $C_{\beta(i)}$–$S_{\gamma(j)}$ = 2.99 ± 0.05 Å and $S_{\gamma(i)}$–$S_{\gamma(j)}$ = 2.02 ± 0.05 Å.

Fifteen slowly exchanging amide protons have been previously identified (Werner & Wemmer, 1991); six additional moderately slowly exchanging amides were identified during the course of this study. Thirteen amide protons were identified as hydrogen-bonded within an antiparallel β-sheet according to the criteria of Wagner et al. (1987). For each of these hydrogen-bonded amides, two additional distance constraints were defined, $N_{(i)}$–$O_{(j)} \leq 3.3$ Å and $NH_{(i)}$–$O_{(j)} \leq 2.3$ Å. Four additional hydrogen bonds involving slowly exchanging amide protons were identified during the course of the refinement by identification of putative hydrogen-bonding partners using interactive graphics and hydrogen-bond analysis using the program DSSP (Kabsch & Sander, 1983).

Constraints on the ϕ angle were classified according to the size of the $^3J_{N\alpha}$ coupling constant (Pardi et al., 1984). For the 29 residues whose $^3J_{N\alpha} \geq 8$ Hz, ϕ was constrained to the range $-80° \leq \phi \leq -160°$; 19 residues had $^3J_{N\alpha} \ll 7$ Hz and were constrained to $-20° \leq \phi \leq -100°$. Constraints on χ_1 were determined on the basis of the criteria of Wagner et al. (1987) by examination of DQF-COSY, P.E.COSY, and 40-ms NOESY spectra in D_2O and H_2O. From this analysis, six were constrained to $0° \leq \chi_1 \leq 120°$, 14 constrained to $0° \leq \chi_1 \leq -120°$, and seven were constrained to $120° \leq \chi_1 \leq 240°$. For the six X–Pro peptide linkages, the four trans ω angles were constrained to 180° ± 6.3°, and the two cis ω angles were constrained to −2.5° ± 16.2° according to Stewart et al. (1990). Valine 52 was found to belong to the g^- rotomer classification (Zuiderweg et al., 1985), and the χ_1 angles involving the methyl groups were defined to be 60° ± 60° and −60° ± 60°.

Stereoassignments were completed for 35 prochiral centers, including the δCH_3's of L29 and the γCH_3's of V52, in a manner analogous to that of Weber et al. (1988).

Calculations. The three-dimensional structure of BBI-I was calculated using a two-stage protocol of dynamical simulated annealing employing the program XPLOR (version 2.1, Brünger et al., 1986, 1987a,b). All calculations were carried out using a Stardent GS2000 computer, and the structures were studied graphically using the program INSIGHT II (Biosym Technologies, Inc.) running on a Silicon Graphics 4D/240GT computer equipped with a Crystal Eyes Stereoscopic Viewing System (StereoGraphics Corp.). A number of recent reports (Nilges et al., 1988a,b,c; Folkers et al., 1989; Driscoll et al., 1989; Clore et al., 1991) have discussed the general methodology of dynamical simulated annealing; thus, only the details relevant to its present application will be presented here.

This study employed a two-stage protocol of dynamical simulated annealing, the first of which "folded" the molecule from a random ϕ and ψ array, and the second of which refined the molecule iteratively as more and more information was input to the calculation. Initially, the molecular structure of BBI-I was defined by the amino acid sequence, and ϕ and ψ angles were chosen using a random number generator with the χ angles left fully extended (180°). A total of 92 initial structures were calculated in this manner and were "folded" using the stage I protocol (Table I). This protocol is essentially that of Nilges and Brünger (1990). During this folding stage, the seven disulfide bonds were introduced by stripping off the hydrogen from the sulfur, reducing the van der Waals radius of the sulfur atom, and applying the distance constraints denoted above rather than explicitly defining the S–S bond. No hydrogen bond constraints were included at this stage, and the two X–Pro cis-peptide linkages (N18–P19 and Y45–P46) identified previously in NOESY spectra (Werner & Wemmer, 1991) were initially defined to be trans to avoid any prior bias in the peptide-bond geometry during the folding stage.

Stage II of the protocol (Table I) employed essentially the protocol of Nilges, Clore, and Gronenborn which was used in the hybrid distance geometry–dynamical simulated annealing approach of these authors (Nilges et al., 1988a,b,c; Clore et al., 1991). This latter protocol was sufficiently robust for refinement of the initially folded structures and required half the computational time of the folding protocol. During this second stage, the S–S bonds for the disulfide linkages were defined explicitly, and the 13 hydrogen bonds of the β-sheets, plus four additional hydrogen bonds, were defined as outlined above. This second stage was repeated several times, each employing further constraints generated through an improved ability to unambiguously assign NOEs by comparing distances in the folded structures from stage I with 60- and 125-ms NOESY spectra. Additional constraints from NOEs observed in 125- and 200-ms NOESY spectra were included after one round of stage II refinement as the structures could be used to verify that the NOEs observed were consistent with these partially refined structures rather than due to spin diffusion. Subsequently, stereoassignments for 35 prochiral centers were included, as were a number of ϕ and χ_1 torsion angle constraints as outlined above.

RESULTS

Effect of Cosolvent. At the outset of this study, it was important to determine to what extent the native protein structure was preserved in the presence of acetonitrile. As discussed in a previous report (Werner & Wemmer, 1991), acetonitrile was found to be essential for the completion of the ^1H NMR assignments due to the inherent self-association of BBI-I. Figure 1 compares the 125-ms NOESY spectra of BBI-I in the presence and absence of acetonitrile. As can be seen in the figure, the pattern of sequential connectivities for the fragment Q21–S25 is identical under both solvent conditions. Most important in this comparison are the relative chemical shift positions in each spectrum and their relative intensities; in both cases, the relative chemical shift within each spectrum is conserved, although there are chemical shift differences between spectra due to the presence of the polar organic solvent. The chemical shift is extremely sensitive to the local environment around any given nucleus, thus, the

Table I: Two-Stage Simulated Annealing Protocol

Stage I: Folding from a Random ϕ/ψ Array[a]	
phase 1: 50 cycles Powell minimization[b]	
k_{NOE}	50 kcal/(mol·Å^2)
k_{TOR}	off
k_{REPEL}	0.002 kcal/(mol·Å^4)
phase 2: 15 ps dynamics at 1000 K[c]	
k_{NOE}	50 kcal/(mol·Å^2)
k_{TOR}	off
k_{REPEL}	0.002 kcal/(mol·rad^4)
phase 3: 1 ps dynamics at 1000 K[d]	
k_{NOE}	50 kcal/(mol·Å^2)
k_{TOR}	off
k_{REPEL}	0.002–0.1 kcal/(mol·rad^4)
phase 4: dynamic cooling to 300 K[e]	
k_{NOE}	50 kcal/(mol·Å^2)
k_{TOR}	50 kcal/(mol·rad^2)
k_{REPEL}	0.1 kcal/(mol·rad^4)
phase 5: 200 cycles Powell minimization	
k_{NOE}	50 kcal/(mol·Å^2)
k_{TOR}	50 kcal/(mol·rad^2)
k_{REPEL}	0.1 kcal/(mol·rad^4)
Stage II: Refinement	
phase 1: 200 cycles Powell minimization[f]	
k_{NOE}	0 kcal/(mol·Å^2)
k_{TOR}	0 kcal/(mol·rad^2)
k_{REPEL}	0 kcal/(mol·Å^4)
phase 2: 3.75 ps dynamics at 1000 K[g]	
k_{NOE}	0.5–50 kcal/(mol·Å^2)
k_{TOR}	0.5–200 kcal/(mol·rad^2)
k_{REPEL}	0.001–0.25 kcal/(mol·Å^4)
phase 3: 1.5 ps dynamic cooling to 300 K[h]	
k_{NOE}	50 kcal/(mol·Å^2)
k_{TOR}	200 kcal/(mol·rad^2)
k_{REPEL}	4 kcal/(mol·Å^4)
phase 4: 200 cycle Powell minimization	
k_{NOE}	50 kcal/(mol·Å^2)
k_{TOR}	200 kcal/(mol·rad^2)
k_{REPEL}	4 kcal/(mol·Å^4)

[a] The values for the force constants for the bond, angle, and improper torsions were set to uniform high values throughout the calculations [600 kcal/(mol·Å^2), 500 kcal/(mol·rad^2), and 500 kcal/(mol·rad^2), respectively]. The usual nonbonded potential of the CHARMM (Brooks et al., 1983) empirical energy function was replaced with the repulsive quartic potential of XPLOR. The "soft square-well" NOE potential was used with the initial asymptote set equal to 0.1. Center averaging was employed throughout for the experimental distance constraints. [b] The experimental torsion force constant (k_{TOR}) was turned off until phase 4 of stage I. [c] The Maxwellian velocity distribution was rescaled every 2 fs to 1000 K. The SHAKE algorithm (Ryckaert et al., 1977) was not employed in stage I. [d] The asymptote of the soft square-well NOE potential energy function was increased by 0.1 every 1 ps to a maximum value of 1.0; k_{REPEL} was simultaneously multiplied by 1.5 to a maximum value of 0.1 kcal/(mol·Å^4). [e] The experimental torsional force constant was included (k_{TOR}), and the NOE potential was switched to a square-well potential. The temperature was lowered every 0.1 ps by 25 K to a final temperature of 300 K. [f] The values for the force constants for the bond, angle, and improper torsions were set to uniform high values throughout the calculations [600 kcal/(mol·Å^2), 500 kcal/(mol·rad^2), and 500 kcal/(mol·rad^2), respectively]. The usual nonbonded potential of the CHARMM empirical energy function was replaced with the quartic repulsive potentiao of XPLOR. Center averaging was employed throughout for the experimental distance constraints. The SHAKE algorithm was employed throughout the dynamics runs with a tolerance of 1×10^{-3}. [g] k_{NOE} was increased to 50 kcal/(mol·Å^2) and k_{TOR} was increased to 200 kcal/(mol·rad) by doubling their values every 75 fs. k_{REPEL} was increased to 0.25 kcal/(mol·Å^4) by multiplying its value by 1.125 every 75 fs. The Maxwellian velocity distribution was rescaled every 75 fs to 1000 K. [h] The temperature was lowered by 25 K every 50 fs and the van der Waals radius scale factor was lowered from 1.0 to 0.8. k_{REPEL} was set to 4 kcal/(mol·Å^4) at the beginning of the phase 3.

preservation of the relative chemical shift positions under both solvent conditions indicates that the basic fold of the peptide backbone is preserved.

Qualitative examination of the relative NOE intensities

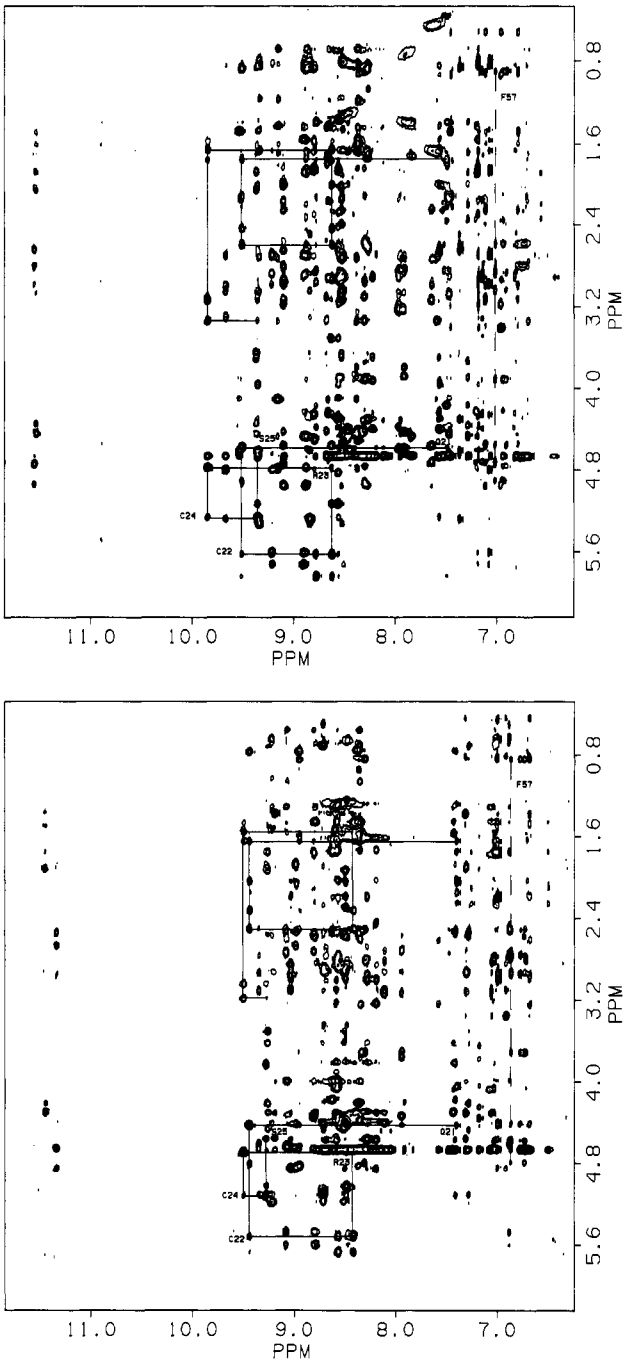

FIGURE 1: 125-ms NOESY spectra of BBI-I (pH 7.3, 25 °C) collected in the presence (a, top) and absence (b, bottom) of acetonitrile. The sequential $d_{\alpha N(i,i+1)}$ and $d_{\beta N(i,i+1)}$ NOEs are traced for the segment Q21–S25 in the antitryptic domain of BBI-I. The NOEs involving the ring δ-protons of F57 are indicated with the dashed line in panels a and b (see Discussion). Note that the δ-protons of F50 and F57 are nearly degenerate in panel b.

within each spectrum again indicates that the basic fold of the backbone is preserved in the cosolvent. For example, the relative intensities for the intraresidue Nα NOE of C22 and the sequential αN(i,i+1) NOE for Q21–C22 are seen to be very different in intensity in Figure 1 (weak and strong intensity, respectively). C22 is known to be in a region of antiparallel β-sheet (Werner & Wemmer, 1991), thus the observed NOE intensities are consistent with the expected intensity pattern for this structural element (Wüthrich, 1986). The entire segment Q21–S25 is in β-sheet conformation and follows this pattern of a strong sequential αN(i,i+1) NOE and a weaker intraresidue Nα NOE in spectra collected both in the presence and absence of acetonitrile.

Secondarily, it is important to compare the NOEs involving side-chain protons as they represent many of the "long-range" NOEs which determine the global fold of the molecule. For example, examination of the amide to methyl (<1 ppm) regions in Figure 1 again indicates that the pattern of NOEs and relative NOE intensities are preserved under both solvent conditions; the same is observed for the NOEs between the aromatic ring protons and other side-chain protons. A more thorough comparison of the two spectra indicates that the pattern of NOEs and their relative intensities are preserved throughout the spectrum for all protons, confirming that the native protein structure is essentially unchanged by the presence of acetonitrile. The difference between spectra collected under the two solvent conditions is primarily the greater chemical shift dispersion in the presence of acetonitrile and the narrowing of resonances in the same spectrum, presumably due to the disruption of the self-association process.

Distance and Angle Constraints and Stereospecific Assignments. A total of 650 NOE distance constraints were derived from one 60-ms NOESY in H_2O (pH 5.7, 35 °C) and one 40-ms NOESY in D_2O (pH 5.7, 35 °C). An additional 257 NOEs were derived primarily from a 200-ms NOESY spectrum (pH 5.7, 35 °C) and a 125-ms NOESY spectrum (pH 5.0, 25 °C) by utilization of the initial family of 53 structures (determined from one cycle of folding and refinement) to resolve ambiguities in the assignment of NOESY spectra. These additional NOEs involved primarily side-chain protons and were very useful in determining the global fold of the molecule, comprising nearly half of the tertiary NOEs assigned in the spectra of BBI-I.

The analysis of torsion angle constraints was complicated by the relatively large line widths, perhaps indicating residual self-association, even in the presence of acetonitrile. The measurement of $^3J_{N\alpha}$ using the method of Kim and Prestegard (1989) requires that the line shape of the measured resonance be Lorentzian; however, in DQF-COSY spectra of BBI-I, the line width of the multiplet components was typically broad, and the line shape could not be fit to a single Lorentzian. In addition, resolution enhancement was necessary in order to resolve the cross peaks in the spectrum. It was found that it was possible to determine wheather a coupling constant was larger than 8 Hz or much smaller than 7 Hz, but an accurate measure beyond this was not possible and probably could not be determined using a cross-peak simulation program. Simulation programs such as the SPHINX-LINSHA package (Widmer & Wüthrich, 1986, 1987) rely on a visual comparison to determine the size of $^3J_{N\alpha}$. Examination of Figure 2 of Werner and Wemmer (1991) indicates that the apparent coupling constants are very similar to one another in DQF-COSY spectra. It was concluded that it would be difficult to properly model the relaxation behavior of the DQF-COSY data due to the influence of the self-association equilibrium; to properly simulate the data, a detailed line-shape analysis would have had to have been done, and it was not considered to be warranted considering the loose ϕ angle constraint interpretation that is possible by measurement of the backbone coupling constant (Pardi et al., 1984). Thus, backbone coupling constants were discriminated using the Kim and Prestegard method (i.e., > 8 Hz or ≪7 Hz), and the ϕ angle constraint was set very conservatively, $-80° \leq \phi \leq -160°$ for $^3J_{N\alpha} \geq 8$ Hz and $-20° \leq \phi \leq 100°$ for $^3J_{N\alpha} \ll 7$ Hz.

The degree of chemical shift degeneracy in the DQF-COSY spectrum of BBI-I also hampered an accurate measurement of the $^3J_{\alpha\beta}$ constant. As can be seen from Figure 1 of Werner and Wemmer (1991), there is substantial α and β chemical shift overlap for many of the upfield cross peaks involving residues of three or greater spins (i.e., $H_\beta < 2.5$ ppm). Thus, in the P.E.COSY spectrum, the overlap of cross peaks precluded the accurate measurement of many of the coupling constants associated with these amino acids. Several cross peaks had multiplet components which were cancelled due to overlap with other cross-peak components opposite in phase from a different residue; other cross peaks were simply in a very crowded region of the spectrum that prevented the accurate identification and measurement of the coupling partners. As a consequence, although it was easy to determine whether the coupling constant was strong (≥7 Hz) or weak (≤5 Hz), it was not possible to measure accurately enough $^3J_{\alpha\beta}$ to incorporate this information with $^3J_{N\alpha}$ into an automated program for stereoassignment of prochiral centers, e.g., HABAS (Güntert et al., 1989) or STEREOSEARCH (Nilges et al., 1990). Thus, stereospecific assignments were done using the best 20 of 53 structures after all the NOEs had been incorporated into the dynamical simulated annealing protocol (i.e., one folding and two refinement stages).

It has been previously shown that stereospecific assignments can be determined by comparing the calculated structures and the NOE data to determine whether a given β-methylene proton ends up at a pro-*R* or a pro-*S* position (Weber et al., 1988). If a proton consistently comes up in a single prochiral position, then the proton can be considered to be assigned stereospecifically. In the present application, a 35-ms NOESY spectrum in H_2O and a 40-ms NOESY spectrum in D_2O (35 °C, pH 5.7) were used to discriminate the intensities of intraresidue Nβ and $\alpha\beta$ NOEs, respectively. The 20 best of 53 structures (as determined by agreement with NOE and ϕ angle constraints) were then examined to see how the intraresidue distance relationships of each clearly resolved β-methylene proton in the calculated structures agreed with the observed NOE intensities. Initially, the NOEs examined in the structures involved protons (not related sequentially) which included only one of the two β-methylene protons in a given residue. If the structures indicated that this "long-range" NOE consistently involved only one of the β-protons, a putative stereoassignment was made. The intraresidue Nβ and $\alpha\beta$ NOE intensities were then evaluated in 40-ms NOESY spectra and compared to the relative strength of the NOE expected from the structures, based on this putative assignment. If both sets of analysis agreed in 80% of the structures, a stereoassignment was considered to have been made and was incorporated into the refinement. In a few cases, the stereoassignment began with interresidue NOEs to both β-protons, which were clearly distinguished in intensity at 40-ms (i.e., one strong and one medium intensity NOE). Subsequently, consistency with the intraresidue NOE intensities expected from the initial structures was looked for prior to making the final assignment, as discussed above. During the last two rounds of refinement, the structures were checked to ensure that the methylene positions did not switch places during the high-temperature phases of the dynamics calculations.

The γCH_3's of V52 and δCH_3's of L29 were assigned stereospecifically following a similar procedure of inter- and intraresidue NOE analysis and comparison with the 20 structures. For V52, the $^3J_{\alpha\beta}$ constant was very small, the intraresidue NH–γCH_3 NOEs were both strong, and the intraresidue Nβ NOE was quite weak by comparison. These observations were all consistent with a g^- rotomer conformation about C_β (Zuiderweg et al., 1985). The asymmetry in the NOE intensities of the α–γCH_3 NOEs confirmed the assignment. The intraresidue Nβ and Nγ NOEs of L43 were

Table II: NOEs Defining Type VIb Turns in BBI-I

antitrypsin	antichymotrypsin
T15NH–P20Hα	L43Hα–A47Hβ
S17NH–T15Hγ	S44NH–A42β
S17NH–P20Hα	S44NH–L43β
S17NH–P20Hβ	S44NH–A47Hα
S17NH–P20Hγ	S44NH–A47β
S17NH–Q21NH	Y45Hα–A47Hα
N18Hα–19Hβ	Y45Hα–P46Hβ
N18Hα–P20Hδ,δ′	Y45Hα–A47Hβ
N18NH–P20Hα	Y45Hβ–P35Hα
P19Hα–N18Hβ	Y45Hδ–A47Hα
P19Hβ–P20Hβ	Y45NH–A47Hα
P19Hβ–P20Hδ	Y45NH–A47NH
	P46Hβ–L29Hδ

unresolved and no stereospecific assignment has been made for them.

The ϕ angle for S25 was found to be +50° ± 20° in 100% of the structures in which all the NOEs had been incorporated. Its backbone coupling constant was found to be moderate to strong (6–8 Hz) and therefore consistent with the empirical Karplus equation relating the coupling constant and the ϕ angle (Pardi et al., 1984). Thus, in the final two rounds of refinement, the ϕ angle for S25 was constrained to be +60° ± 40°. C58 was also found to have a positive ϕ angle in 80% of the structures after three rounds of refinement and the same range for its ϕ was incorporated during the last round of refinement.

Description of the Tertiary Structure. The structure of BBI-I is comprised of two distinct domains, one capable of inhibiting chymotrypsin (residues 27–53, Figure 2c,d) and a second capable of inhibiting trypsin (residues 7–26 and residues 54–63, Figure 2a,b). Each inhibitory domain is characterized by a β-hairpin comprised of five residue pairs of antiparallel β-sheet and a five-residue type VI reverse turn containing a cis X–Pro peptide bond (N18–P19 and Y45–P46 in the antitryptic and antichymotryptic domains, respectively). Both type VI turns could be classified as type VIb according to the criterion of Richardson (1981).

The antitryptic domain hairpin extends from residues Q11–S25. The plane of the β-sheet is quite planar and extended (Figure 3b), each strand of which is held in place by the disulfide cross-link across the sheet (C14–C22) as well as the cross-links from each strand to the rest of the antitryptic domain (C9–C24 and C12–C58).

In the tryptic inhibitory domain, the type VIb turn includes residues K16–P20, with the P_1–P_1' reactive site for trypsin at the peptide bond K16–S17. The turn was defined by a number of (i,i+1) and (i,i+2) NOEs (Table II) involving both backbone and side-chain atoms. No hydrogen bond (i,i+3) was identified across the loop (which is common to type I and type II turns), due to the presence of proline at the (i+3) position in the loop. There were few constraints identified for the side-chain atoms of K16–N18; thus their side-chain positions are poorly defined beyond C_β (Figure 2b). Characteristic of other serine protease inhibitor families (Laskowski & Kato, 1980), this domain contains a disulfide cross-link proximal to the reactive site for trypsin (C14–C22) which presumably maintains a rigid combining site for serine protease (see Discussion).

The tryptic inhibitory domain also contains a short third strand of antiparallel β-sheet between residues I54 and D56, hydrogen-bonded to residues Q21–R23. Two half-turns lead into and out of the hairpin in the antitryptic domain, C9–Q11 and S25–M27, the former being defined by the NOE C9α–Q11NH. The near degeneracy of the chemical shifts of the H_α's of M27 and K37 precluded the unambiguous observation of the NOE M27α–S25NH which would have defined this half-turn.

In the chymotrypic inhibitory domain, the β-hairpin includes residues S38–V52 with the type VIb turn comprising residues L43–A47. Again, a number of NOEs defined the turn, as delineated in Table II. The turn of the β-hairpin is twisted slightly (Figure 3b), constrained in part by the observation of an NOE between the H_β of P46 and the δCH_3 of L29. The twist in the type VIb turn is consistent with the observation of the relatively small $^3J_{N\alpha}$ ($\ll$7 Hz) of residues A42 and A47 and their correspondingly weaker sequential NOEs. In contrast to the antitryptic domain, a relatively weak hydrogen bond is observed closing this loop between A47NH and S44CO. The characteristic cross-link proximal to the reactive site loop occurs between C41 and C49 in this domain. Each strand of the hairpin sheet is held in place by the cross-links C32–C39 and C36–C51.

A short antiparallel triple-stranded region also occurs in this domain, including residues M27–L29, opposite Q48–F50. Two half-turns also lead into and out of the β-hairpin of this domain, C36–S38 and V52–I54. The former defined by an NOE (i,i+2) $H_\alpha N$, whereas the latter was not defined by any NOEs specifically between backbone atoms.

The Converged Structures. Of 92 random ϕ/ψ coordinate arrays, 53 converged to a family of structures having the same basic global conformation after a single folding and a single refinement simulated annealing run. The second round of refinement incorporated secondary and tertiary NOEs derived from 125- and 200-ms NOESY spectra, as discussed above. The structures were then examined in conjunction with the NOESY spectra, and stereoassignments were made for 35 prochiral centers. These stereoassignments were incorporated into the calculation, and all 53 structures were refined in the third round. The fourth round consisted of inclusion of the ω and χ_1 torsion constraints for all 53 structures, and the final round included only the 32 structures which best satisfied the experimental constraints, correcting misassignments and typographical errors in the NOE list. The positive ϕ angle constraints noted above were also included in these latter stages. Sixteen structures were chosen as comprising the best family of converged structures, based on their low NOE and TORSION energies and low number of poor nonbonded contacts.

Table III summarizes the agreement with experimental constraints and the structural energetics for the best 16 simulated annealing structures. As can be seen from the table, there is good agreement with the observed NOEs for all three classes of experimental constraints. Deviations from torsional constraint limits are also very small, but, considering the wide ranges allowed for them, this is would be expected.

Although residues 1–6 and 64–71 were included throughout the calculations, they have not been included into the analysis of Table III due to the lack of any long-range NOEs which would have defined their conformation relative to the rest of the molecule. The complete lack of any nonsequential interresidue NOEs implies that the structure in the termini is irregular. As a consequence, these residues will be ignored throughout the following discussion.

The RMSD relative to the mean structure derived from the family of 16 indicates that the structure is reasonably well defined, both for the backbone and side chains. It is interesting that the individual domain conformations seem to be better defined when considered independently. As noted in Table III, the RMSD values for the backbone and all atom superpositions are significantly lower for the individual domains. Figure 2 shows the individual domains with and without side

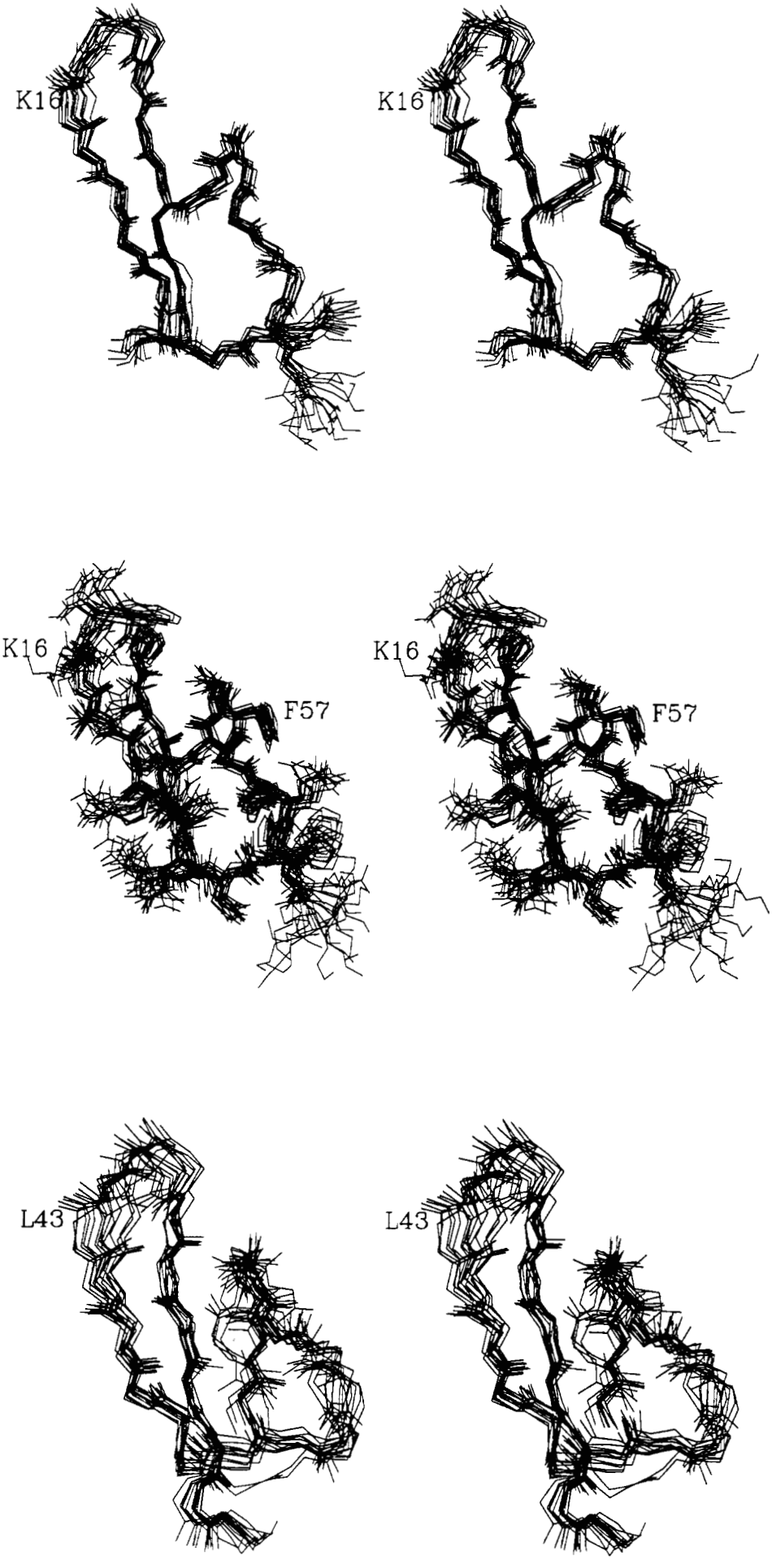
K16
K16
K16
F57
K16
F57
L43
L43

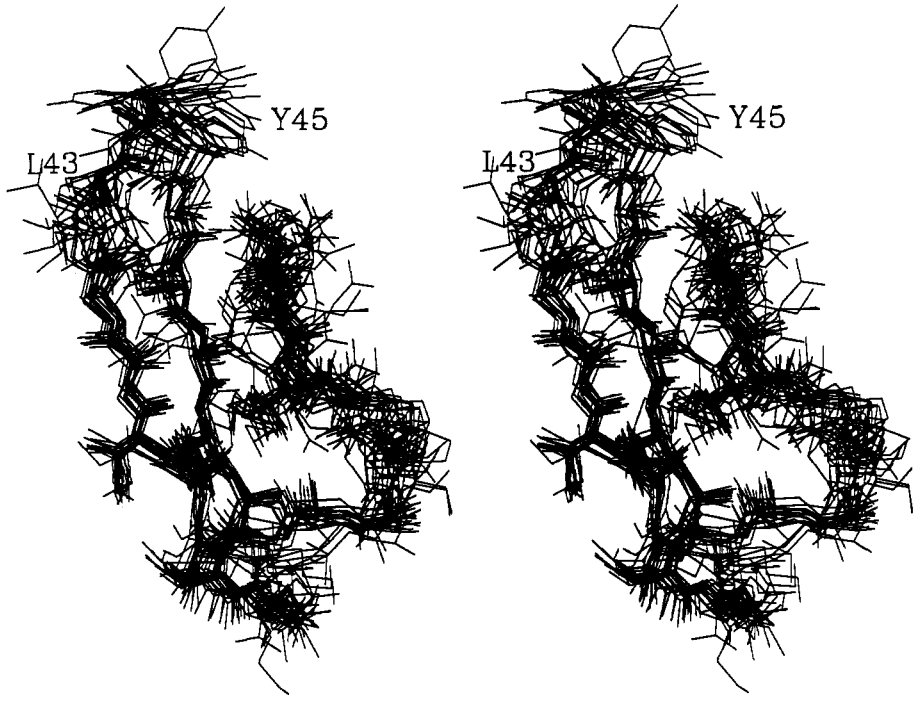

FIGURE 2: Stereodiagram of the 16 superimposed converged structures of the individual inhibitory domains. Backbone atoms are shown for the antitryptic domain (a, opposite page, top) and antichymotryptic domain (c, opposite page, bottom), the same with side-chain atoms in panels b (opposite page, middle) and d (this page), respectively. Several residues are indicated in each domain as discussed in the text.

chains. The lower RMSD values for the individual domains reflects the paucity of tertiary NOEs between segments of the two domains which would have better defined the relationship between them (see Discussion).

Figure 3 shows a superposition of backbone atoms for the converged structures. The regions of antiparallel β-sheet are quite well defined; however, the type VIb turns at one end of each domain hairpin are less well defined (Figure 3b). This is primarily due to the variation in the ψ angle, particularly in the reactive loops (K16–S17 and L43–S44). Although several NOEs defined each of these turns (Table II), there were few constraints which restrained all the backbone torsional parameters, compared to the regions of sheet within the hairpins. This is particularly true for L43–S44 where there were very few NOEs which were observed that constrained L43 to a narrow range of conformational space (Table II).

It is also seen in Figures 2 and 3 that the antichymotryptic domain loop, M27–K37, is less well-ordered in the converged structures than other regions. Although many NOEs between backbone and side-chain atoms were observed for these residues, few of them involved contacts with residues separated by more than one or two amino acids in the primary sequence. In addition, fewer torsional constraints and stereospecific assignments could be defined for these residues relative to those in the hairpins or type VIb turns. As a consequence, this region is the least well defined overall, for both the backbone and side-chain atoms.

Figure 4 illustrates the backbone and all atom RMSD values as a function of residue number of residues 7–63. As can be seen in the figure, the RMSD for the backbone atoms is quite uniform for residues 7–63, but the side chains show much more variability, partly due to the lack of information about torsional parameters, as discussed below.

The Ramachandran plot for residues from all 16 structures (excluding the termini, Figure 5) shows that the converged structures lie primarily in the energetically favorable regions of the Ramachandran map, with a preponderance of residues in the region indicative of β-sheet, consistent with the NOE information which determined the secondary structure of BBI-I (Werner & Wemmer, 1991). It is interesting that the proline residues cluster around $\phi \approx -60°$. No ϕ angle constraint was incorporated for the proline residues during the course of the calculations.

Discussion

The Converged Structures. Overall, the converged structures are quite well defined, despite the variation of some structural parameters in the type VIb turns and in the antichymotryptic domain loop (M27–K37). In spite of the relatively low RMSD for the backbone atoms of residues 7–63, the relationship between the two domains is not as well defined as is the structure within each domain. This can be seen in Figure 6, which shows a superposition of structures using the atoms of each domain separately. As can be seen in the figure, the relationship between the two domains is poorly defined, which accounts for the dispersion in the nonsuperimposed domain. Figure 7 illustrates the lack of NOEs involving backbone atoms in the interdomain region that could have better defined the spatial orientation of the two domains relative to each other.

The larger variation in structure observed in the antichymotryptic domain may reflect fewer stabilizing tertiary interactions within that domain relative to the tryptic inhibitory domain. This may be correlated with the larger loss in inhibitory activity when the antitrypsin and antichymotrypsin domains are proteolytically separated; the tryptic inhibitory domain retains 80% of its activity, while the chymotryptic inhibitory domain retains only 20% activity (Odani & Ikenaka, 1978). If indeed the the antichymotryptic domain is stabilized by fewer internal contacts, then cleavage of the peptide bonds M27–R28 and D56–F57 could lead to further loss of order, reflected in the lower binding affinity for chymotrypsin in the isolated domain.

The NOESY spectra in Figure 1 clearly demonstrate that there is relatively little effect of acetonitrile on the tertiary fold. Examination of the residue solvent accessibilities (Figure 4)

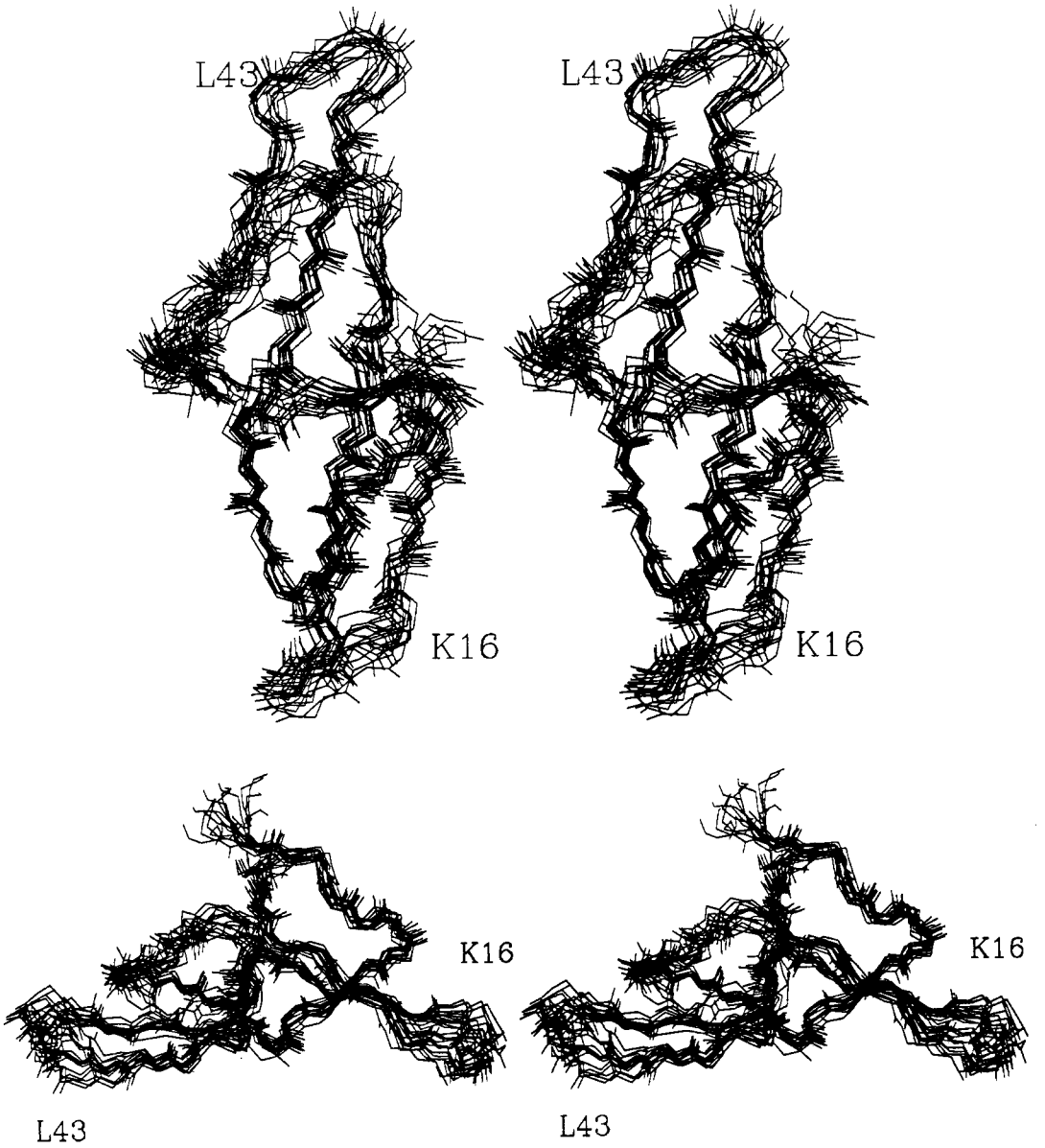

FIGURE 3: Stereodiagram showing the backbone atoms of the 16 converged structures of BBI-I superimposed (residues 7–63). The reactive site (P_1) residue is indicated for each inhibitory domain. (a, top) Top view of both domains, the two termini coming out of the page. (b, bottom) Side view showing the similarity in the conformation of the two domains.

indicates that all of the nonpolar residues have moderately low solvent accessibilities, with the exception of F57, which has a mean solvent accessibility of 137 Å^2 ± 6 Å^2 for the 16 converged structures. This appears to be relatively high for a phenylalanine residue; however, its exposure does not appear to be due to the presence of organic solvent. Examination of the spectra in Figure 1 and a more detailed examination of additional spectra, collected under varying conditions of pH in the absence of acetonitrile, do not indicate a change in pattern or number of observed NOEs involving the ring of F57. The ring appears to be in a pocket which provides little restraint on the position of the side chain (Figure 2b). In addition, the ring of Y58 is close by and the two rings are oriented perpendicular to one another. Perhaps these factors help to stabilize the ring of F57 in a more "solvent-exposed" region of the protein. As noted by Bode and Huber (1991), it is quite common to find nonpolar residues with relatively high solvent accessibilities in many of the small serine protease inhibitor families.

The P_1–P_1' reactive site of each domain is part of a bulge in the type VIb turn of the hairpin. These bulges show the greatest variability in local conformation, largely due to the lack of NOE observations providing long-range constraints. The turn in each domain appears to be fully exposed to solvent, with the antichymotryptic domain including exposed tyrosine and leucine residues. This region is presumably the location of the self-association surface of BBI-I. Harry and Steiner (1969) previously determined that the self-association surface is likely to be nonpolar since the apparent self-association equilibrium constant doubled with a 10-fold increase in salt concentration. A related inhibitor from soybeans, PI-II, was found to form dimers of trimers in the asymmetric unit of protein crystals (Chen, 1989). The second trypsin inhibitory domain of PI-II (analogous to the chymotryptic inhibitory domain of BBI-I) had numerous crystal contacts between protein molecules in the trimers, in support of the notion that the antichymotryptic domain is the location of the self-association surface in BBI-I.

Although there are numerous NOEs involving the backbone atoms of each type VIb turn (Table III), relatively few involve either K16 or L43. The ψ angle variability contributes in large part to the dispersion in the plane of the turns, exemplified

Table III: Structural Statistics for BBI-I[a]

Deviations from Experimental Constraints[b]	
intraresidue (328)	0.182 ± 0.07 Å
sequential (206)	0.147 ± 0.1 Å
secondary and tertiary (373)[c]	0.155 ± 0.14 Å
ϕ (38)[d]	3.3° ± 5.7°
χ^1 (29)[d]	4.6° ± 9.5°
number of violations ≥0.5 Å	
intraresidue	0
sequential	1
secondary and tertiary	4
Energetics[b]	
F_{NOE} (kcal·mol^{-1})	56.2 ± 22.1
$F_{TORSION}$ (kcal·mol^{-1})	15.7 ± 14.3
F_{REPEL} (kcal·mol^{-1})	40.9 ± 9.8
$E_{L\text{-}J}$ (kcal·mol^{-1})[e]	−225.6 ± 13.4
Mean RMS Deviations from Idealized Geometry	
bonds (Å)	0.0104
angles (deg)	2.33
impropers (deg)	0.388
Atomic RMS Differences (Å)[f]	
both domains (7–63)	
backbone	1.01 ± 0.15
all atoms	1.36 ± 0.19
antitryptic (7–62, 54–63)	
backbone	0.70 ± 0.12
all atoms	1.00 ± 0.12
antichymotryptic (27–53)	
backbone	0.82 ± 0.18
all atoms	1.31 ± 0.30

[a] Structural statistics are compiled for residues 7–63, inclusive, unless otherwise noted. No tertiary NOEs were observed for residues 1–6 and 64–71. [b] The force constant for the calculation of the square-well NOE potential energy was set to 50 kcal/(mol·Å^2) and for the calculation of deviation from experimental constraints was set to 10 kcal/(mol·Å^2). The force constant for the calculation of the TORSION potential energy was set to 200 kcal/(mol·rad^2) and that for the calculation of the quartic REPEL potential energy was set to 4 kcal/(mol·rad^4) with the hard-sphere van der Waals radii set to 0.8 times the standard value used in the CHARMM (Brooks et al., 1983) empirical energy function. Uncertainties in NOE deviations and energy values are reported as mean deviations for the 16 converged structures ± one standard deviation. [c] Secondary and tertiary NOEs comprise all nonsequential interresidue NOEs, including those defining the disulfide cross-links and hydrogen-bond constraints as outlined under Materials and Methods. [d] Deviations in ϕ constraints are calculated for residues 7–63 only. Constraints were included in the calculations for residues 2–6 and 66–69, but the structure in the termini was not defined by any NOEs between residues; thus, there are large violations in the backbone ϕ angle for these residues. Violations in the torsional constraints are reported as the mean value of the deviation for the 16 converged structures ± one standard deviation. [e] $E_{L\text{-}J}$ is the Lennard-Jones van der Waals energy calculated with the XPLOR energy function. The hard-sphere van der Waals radii were set to 0.8 times the standard value used in the CHARMM empirical energy function. The Lennard-Jones potential was not incorporated into the simulated annealing calculations. [f] Atomic RMS differences were determined relative to the mean structure calculated from the family of 16 converged structures. "Backbone" refers to all backbone atoms, inclusive of H_α and HN while "all atoms" includes all non-hydrogen atoms for the indicated residues.

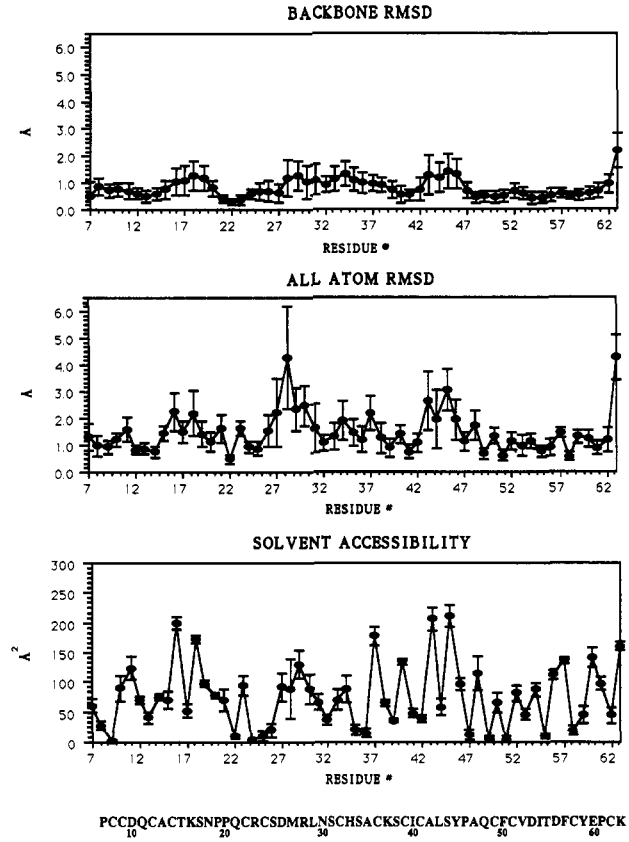

FIGURE 4: Summary of mean backbone and all atom RMSD per residue and solvent accessibility per residue for residues 7–63 of BBI-I. Error bars indicate one standard deviation from the mean. The sequence of residues 7–63 appears at the bottom of the figure.

in Figure 3. In the antichymotryptic domain, Y45 has only one interresidue NOE involving the ring (Table II), constraining it to fold back over the hairpin, albeit in a poorly defined conformation.

Comparison to Other BBI Structures. Several structures of trypsin/trypsin Bowman–Birk inhibitors from other leguminous sources have appeared in the literature. However, neither the structure of inhibitor A-II from peanut (Suzuki et al., 1987) nor the structure of trypsin-bound inhibitor AB-I from azuki bean (Tsunogae et al., 1986) indicated the presence of any regular secondary structure, in stark contrast to that observed for BBI-I. Perhaps further refinement of the structures reported by these authors can resolve the apparent differences between the Bowman–Birk-type inhibitors they have studied and BBI-I.

Chen (1989) has studied the structure of the trypsin/trypsin inhibitor PI-II from soybeans. PI-II is a smaller molecule, having only 65 residues, but it retains the conserved pattern of disulfide cross-links found in all known Bowman–Birk inhibitors. As noted earlier (Werner & Wemmer, 1991), PI-II and BBI-I are quite similar to each other with respect to the β-hairpin of each inhibitory domain. The most significant difference at the level of secondary structure was found to be the shorter trypsin inhibitory hairpin in the N-terminal domain (domain I) of PI-II when compared to the trypsin inhibitory hairpin of BBI-I; in PI-II, the sheet of the hairpin is reduced by two residue pairs.

The hydrogen-bonding pattern within regions of β-sheet is very similar between the two structures. However, significant differences are observed in both type VIb turns and in the loop region of the antichymotryptic domain of BBI-I (M27–K37). In the type VIb turn of domain I of PI-II, crystal data indicate that a hydrogen bond exists between T14CO and S16NH (T15 and S17 in BBI-I). The same is observed between T40CO and S42NH in the second antitryptic domain of PI-II (A42 and S44 in BBI-I). A true hydrogen bond is not believed to exist between these positions in BBI-I; neither the amide proton of S17 nor S44 is slowly exchanging, both having a half-life shorter than 60 min at pH 4.6, 25 °C, for ^{1}H–^{2}H exchange. If hydrogen bonds existed involving these two amide protons, both would exhibit a significantly longer half-life under these conditions.

In PI-II, the main-chain amide protons of residues D9, Q20, K35, and Q46 are involved in hydrogen bonds to side-chain oxygens. Of the analogous residues in BBI-I, only Q21 and

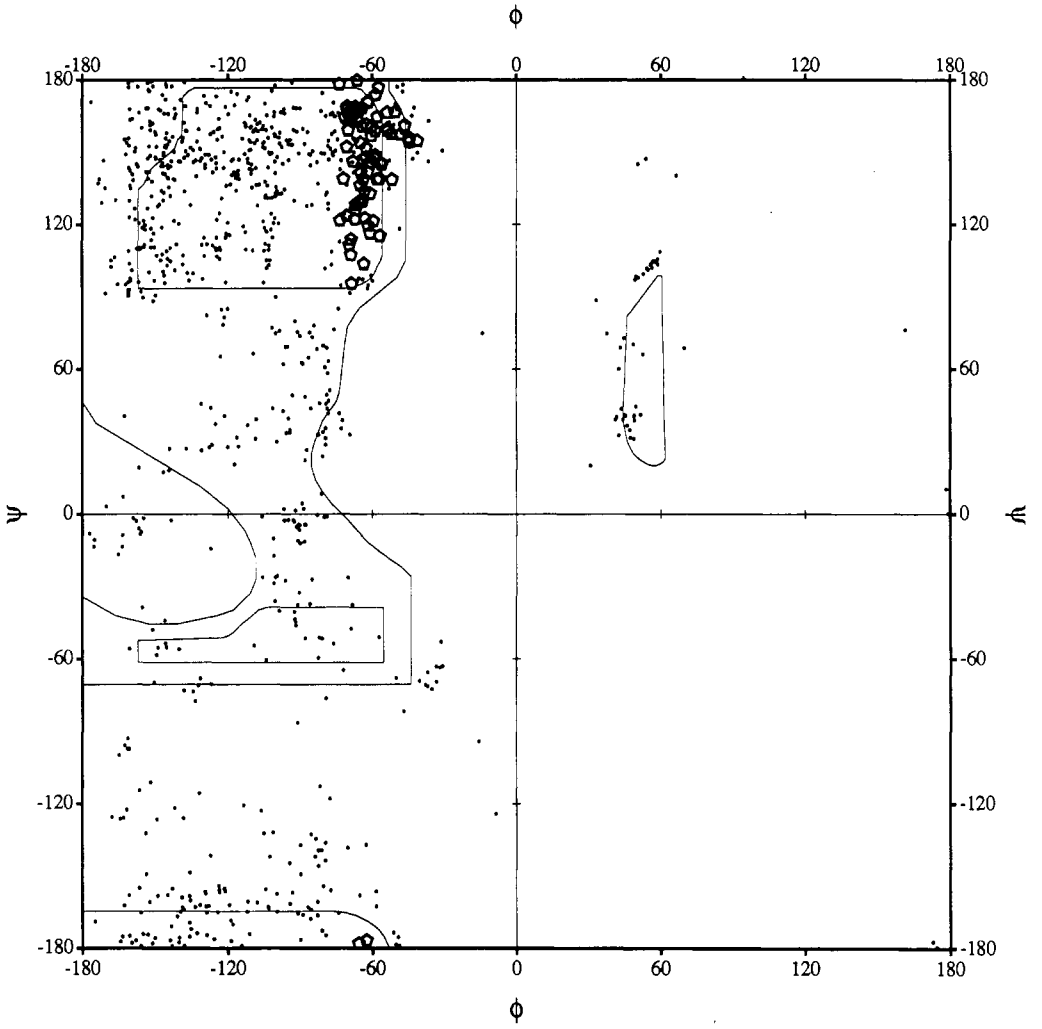

FIGURE 5: Ramachandran plot for residues 7–63 for the 16 converged structures of BBI-I. A line is drawn around the most energetically favorable regions of the plot. The proline residues are indicated with small pentagons. All non-proline residues appear as filled dots.

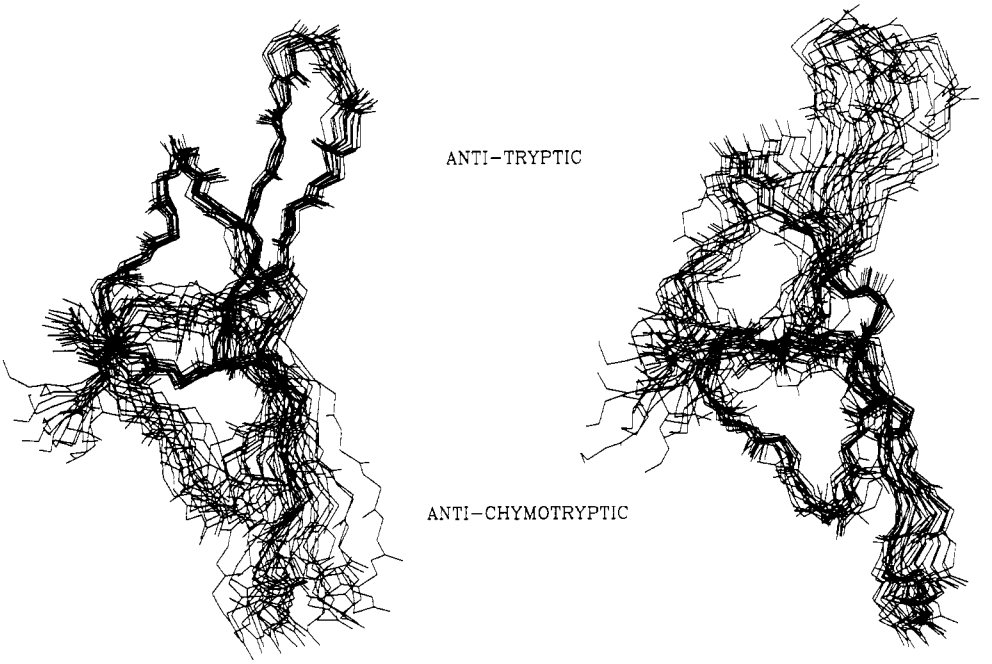

FIGURE 6: Comparison of the the backbone atoms (residues 7–63) for BBI-I when only the atoms of one domain are utilized for superposition. The relative location of the two inhibitory domains is indicated in the figure. The superposition using the tryptic inhibitory domain is on the left and that using the chymotryptic inhibitory domain appears on the right.

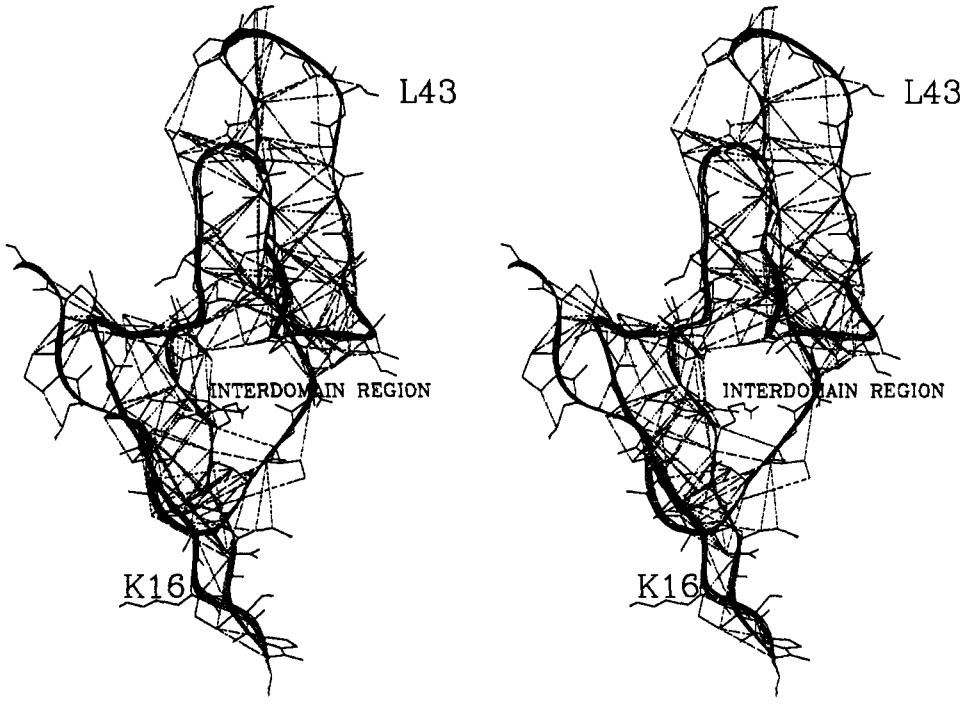

FIGURE 7: Secondary and tertiary NOEs observed for BBI-I. The structure shown is the average structure calculated from the family of 16. The smooth ribbon represents the backbone of the protein for residues 6–64. Dashed lines indicate observed NOEs. Several regions are indicated, as discussed in the text.

Q48 are found to be slowly exchanging. A42 of BBI-I is threonine in PI-II, and it is the threonine side-chain hydroxyl (T40) that is believed to form the hydrogen bond to Q46NH. For Q48 of BBI-I (Q46 in PI-II), the only possible hydrogen-bonding partner is A42, thus the hydrogen bond in BBI-I involves only main-chain atoms. In BBI-I, threonine and glutamine are present at positions 15 and 21, respectively, and Q21 is slowly exchanging; in PI-II, threonine and glutamine occupy the analogous positions 14 and 20. In BBI-I, we believe the hydrogen-bonding partner is the main-chain carbonyl of residue 15 rather than the side-chain hydroxyl as reported for PI-II. Test calculations incorporating a hydrogen bond to the side-chain instead of the main chain oxygen distorted the geometry in the type VIb turn of this domain. Examination of structures calculated without this hydrogen-bond constraint consistently indicated that the main-chain carbonyl was the more likely candidate for hydrogen-bond formation with Q21NH, the main-chain carbonyl being nearly 1 Å closer to Q21NH than the side-chain hydroxyl of T15.

Despite these differences, the overall fold of BBI-I and PI-II are found to be basically the same. Superposition of the C_α coordinates of the two molecules (Chen, Rose, and Wang, personal communication) indicated that the structures in the crystal and in solution were very similar, having an RMSD of approximately 2.1 Å for analogous C_α positions. This is quite reasonable considering that PI-II is six residues shorter in sequence.

Comparison to Other Protease Inhibitor Families. BBI-I shares many features common to several serine protease inhibitor families. The reactive site peptide bond in BBI-I loops out from the type VIb turns, making them accessible to the active sites of trypsin and chymotrypsin. This feature is also observed in PI-II, the Kunitz inhibitor family, and the Kazal inhibitor family. The pointed shape of the type VIb turns reflects also the "lock-and-key" motif believed to be the mode of binding of the serine protease inhibitors to their cognate proteases (Laskowski & Kato, 1980). The turn conformation seems to be optimally oriented for fitting into the active site of the enzyme with the reactive site peptide bond fully accessible to interaction with the active site of the enzyme.

There are some significant differences between the Bowman–Birk inhibitor family and other serine protease inhibitor families. Most notable is the addition of the disulfide cross-link across the β-hairpin in each inhibitory domain. While it is relatively common for there to be a disulfide cross-link proximal to the reactive site, in BBI-I there exists, for example, not only the disulfide cross-links C12–C58 and C9–C24 to each β-hairpin strand in the tryptic inhibitory domain but also the hairpin cross-link C14–C22. In other inhibitor families, the cross-link typically links only the strand on the amino side (P side) of the reactive loop.

Among the small serine protease inhibitor families, it is common for disulfide bonds to link the residues flanking the reactive site loop to a hydrophobic core in the molecule (Bode & Huber, 1991). In contrast, BBI-I does not seem to possess such a core. Indeed, the mean residue solvent accessibility of nonpolar amino acids (valine, leucine, isoleucine, alanine, and phenylalanine) is 87 Å^2 (75 Å^2 if L43 is excluded). As noted above, we do not feel that this is due to the presence of acetonitrile as the NOESY spectra are essentially the same under both solvent conditions (Figure 1). Instead, the disulfide cross-links appear to play more of a role in orienting the inhibitory domains in the proper conformation for binding to serine protease.

Recent experiments measuring amide proton exchange in BBI-I/chymotrypsin complexes indicate significant slowing of exchange rates (relative to free inhibitor) for most of the residues in the antichymotryptic domain (unpublished observations). Work is in progress to examine these exchange rate differences, which will be used in conjunction with molecular modeling, to better understand how BBI-I interacts with serine protease and to study the similarities and differences between BBI and other serine protease inhibitor families.

In conclusion, the three-dimensional structure of soybean trypsin/chymotrypsin Bowman–Birk inhibitor has been determined in solution using two-dimensional ^{1}H NMR spec-

troscopy and dynamical simulated annealing. The coordinates for the family of 16 converged structures and for the refined average structure have been deposited with the Brookhaven Protein Data Bank. A complete list of experimental constraints is available from the authors upon request.

ACKNOWLEDGMENTS

We are grateful to Dr. Steven Muskal for many stimulating discussions and for technical assistance during the course of this study.

REFERENCES

Bode, W., & Huber, R. (1991) *Curr. Opin. Struct. Biol. 1*, 45–52.

Bodenhausen, G., Vold, R. L., & Vold, R. R. (1980) *J. Magn. Reson. 37*, 93–106.

Brooks, B. R., Bruccoleri, R. E., Olafson, B. D., States, D. J., Saminathan, S., & Karplus, M. (1983) *J. Comput. Chem. 4*, 187–217.

Brünger, A. T., Clore, G. M., Gronenborn, A. M., & Karplus, M. (1986) *Proc. Natl. Acad. Sci. U.S.A. 74*, 4130–4134.

Brünger, A. T., Kuryan, J., & Karplus, M. (1987a) *Science 235*, 458–460.

Brünger, A. T., Clore, G. M., Gronenborn, A. M., & Karplus, M. (1987b) *Protein Eng. 1*, 399–406.

Chen, P. (1989) Ph.D. Thesis, University of Pittsburgh, Pittsburgh, PA.

Clore, G. M., Gronenborn, A. M., Nilges, M., & Ryan, C. A. (1987) *Biochemistry 26*, 8012–8023.

Clore, G. M., Wingfield, P. T., & Gronenborn, A. M. (1991) *Biochemistry 30*, 2315–2323.

Driscoll, P. C., Clore, G. M., Beress, L., & Gronenborn, A. M. (1989) *Biochemistry 28*, 2178–2187.

Drobny, G., Pines, A., Sinton, S., Weitekamp, D., & Wemmer, D. E. (1978) *Proc. Chem. Soc. Faraday Symp. 13*, 49–55.

Folkers, P. J. M., Clore, G. M., Driscoll, P. C., Dodt, J., Köhler, S., & Gronenborn, A. M. (1989) *Biochemistry 28*, 2601–2617.

Güntert, P., Braun, W., Billeter, M., & Wüthrich, K. (1989) *J. Am. Chem. Soc. 111*, 3997–4004.

Harry, J. B., & Steiner, R. F. (1969) *Biochemistry 8*, 5060–5064.

Jeener, J., Meier, B. H., Bachmann, P., & Ernst, R. R. (1979) *J. Chem. Phys. 71*, 4546–4553.

Kabsch, W., & Sander, C. (1983) *Biopolymers 22*, 2577–2637.

Kim, Y., & Prestegard, J. H. (1989) *J. Magn. Reson. 84*, 9–13.

Laskowski, M., Jr., & Kato, I. (1980) *Annu. Rev. Biochem. 49*, 593–626.

Macura, S., & Ernst, R. R. (1980) *Mol. Phys. 41*, 95–117.

Marion, D., & Wüthrich, K. (1983) *Biochem. Biophys. Res. Commun. 113*, 967–974.

Mueller, L. (1987) *J. Magn. Reson. 72*, 191–196.

Nilges, M., & Brünger, A. T. (1990) XPLOR *Manual version 2.1*, 260–263.

Nilges, M., Gronenborn, A. M., Brünger, A. T., & Clore, G. M. (1988a) *Protein Eng. 2*, 27–38.

Nilges, M., Clore, G. M., & Gronenborn, A. M. (1988b) *FEBS Lett. 229*, 317–324.

Nilges, M., Clore, G. M., & Gronenborn, A. M. (1988c) *FEBS Lett. 239*, 129–136.

Nilges, M., Clore, G. M., & Gronenborn, A. M. (1990) *Biopolymers 29*, 813–822.

Odani, S., & Ikenaka, T. (1978) *J. Biochem. (Tokyo) 83*, 747–753.

Pardi, A., Billeter, M., & Wüthrich, K. (1984) *J. Mol. Biol. 180*, 741–751.

Plateau, P., & Guéron, M. (1982) *J. Am. Chem. Soc. 104*, 7310–7311.

Redfield, A. G., & Kunz, S. D. (1975) *J. Magn. Reson. 19*, 250–254.

Richardson, J. S. (1981) *Adv. Protein Chem. 34*, 167–339.

Ryckaert, J.-P., Ciccotti, G., & Berendsen, H. J. C. (1977) *J. Comput. Phys. 23*, 327–341.

Stewart, D. E., Sarkar, A., & Wampler, J. E. (1990) *J. Mol. Biol. 214*, 253–260.

Suzuki, A., Tsunogae, Y., Tanaka, I., Yamane, T., Ashida, T., Norioka, S., Hara, S., & Ikenaka, T. (1987) *J. Biochem. (Tokyo) 101*, 267–274.

Tsunogae, Y., Tanaka, I., Yamane, T., Kikkawa, J.-I., Ashida, T., Ishikawa, C., Watanabe, K., Nakamura, S., & Takahashi, K. (1986) *J. Biochem. (Tokyo) 100*, 1637–1646.

Wagner, G., Braun, W., Havel, T. F., Schaumann, T., Go, N., & Wüthrich, K. (1987) *J. Mol. Biol. 196*, 611–639.

Weber, P. L., Morrison, R., & Hare, D. (1988) *J. Mol. Biol. 204*, 483–487.

Werner, M. H., & Wemmer, D. E. (1991) *Biochemistry 30*, 3356–3364.

Widmer, H., & Wüthrich, K. (1986) *J. Magn. Reson. 70*, 270–279.

Widmer, H., & Wüthrich, K. (1987) *J. Magn. Reson. 74*, 316–336.

Wüthrich, K. (1986) *NMR of Proteins and Nucleic Acids*, Wiley, New York.

Wüthrich, K., Billeter, M., & Braun, W. (1983) *J. Mol. Biol. 169*, 949–961.

Zuiderweg, E. R. P., Boelens, R., & Kaptein, R. (1985) *Biopolymers 24*, 601–611.